Numerical Simulations of Shock/Vortex Interaction in Non-Circular Jets

Zonglin Jiang[1] and Kazuyoshi Takayama[2]

[1] LHD, Institute of Mechanics, Chinese Academy of Sciences, Beijing 100080, China
[2] Shock Wave Research Center, Institute of Fluid Science, Tohoku University
2-1-1 Katahira, Aoba-ku, Sendai 980-8577, Japan

Abstract. In this paper, a numerical study of self-induced flow motions of non-circular jets is described to investigate the underlying mechanism of shock/vortex interaction, and axis-switching of the primary vortex loop in its initial stage. Numerical results were obtained by solving three-dimensional Euler equations with a dispersion-controlled scheme and displayed in the form of iso-vorticity surfaces. From the results, it was concluded that secondary flows, secondary shock waves and axis-switching play an important role in the jet instability development, and these are also the primary driving forces leading to the generation of hairpin vortices and complex coherence structures.

1 Introduction

Jets are widely applied in various industrial devices, e.g. rocket launching, fuel/air mixing and thrust producing in aircraft engines. Extensive investigations have been made on both planar and axisymmetric jets to enhance mixing process and thrust production or to reduce screech tones in nozzle flows. It is well known that non-circular jets are more unstable than two-dimensional ones (Krothapalli et al. 1981). This is not only because the non-circular jets have large-scale coherent structures and streamwise vortices, but also because of its special features, such as three-dimensional shock/vortex interactions, asymmetrical vorticity distributions and axis-switching (Husain and Hussain 1993, Koshigoe et al. 1989, and Tam and Thies 1993). Recently, there has been a growing interest in the use of non-circular jets in high-speed propulsive systems (Raman and Taghavi 1998). In such the systems, the residence time of air in hypersonic airplane engines is on order of 1 *ms* for typical flight conditions. Within this short time, the fuel must be injected, and penetrate deeply into air-stream, and be fully mixed for high quality combustion. Non-circular jets can offer possibilities of mixing process enhancement. The relevant research of axis switching and shock-enhanced mixing process have been reported by Krothapalli et al.1981 and Lee et al. 1998, but their research is mainly limited to either experimental measurements of average jet properties or theoretical analysis of jet instability models. The objective of this paper is to numerically investigate into the initial deformation of the primary vortex loop and the development of non-circular jet flows to explore the origin resulting in axis-switching and jet instability.

One way to study non-circular jets in laboratory is discharging a transmitting shock wave from the open end of a rectangular shock tube into ambient air

(Onodera et al. 1998). The primary vortex loop which develops near the open end of the shock tube behind the transmitting shock wave takes the shape of the shock tube cross section and is planar, but deforms quickly into a three-dimensional configuration. Three-dimensional secondary shock waves will also develop later for supersonic jets. This shock/vortex interaction will result in additional flow instability on the shear layer.

In order to remove uncertain factors and focus our attention on shock/vortex interaction and axis-switching, jet flows in the present study are assumed to be symmetrical and viscosity effects on the motion of the primary vortex loop at its early stage are negligible. Numerical simulations were carried out by solving the three-dimensional Euler equations with a dispersion-controlled scheme (Jiang et al. 1995). Four cases presented are of similar geometries with square or rectangular cross-sections, but with different aspect ratio and Mach number. The flow spreading, the secondary flow motion, the secondary shock wave generation, axis-switching, and aspect ratio effects on axis-switching are discussed in detail.

2   Governing Equations

Under the assumption mentioned in the above section, a hyperbolic system of three-dimensional conservation law for a perfect gas in Cartesian coordinates can be written as

$$\frac{\partial \mathbf{U}}{\partial t} + \frac{\partial \mathbf{F}}{\partial x} + \frac{\partial \mathbf{G}}{\partial y} + \frac{\partial \mathbf{E}}{\partial z} = 0, \tag{1}$$

where $\mathbf{U}$, $\mathbf{F}$, $\mathbf{G}$ and $\mathbf{E}$ denote the state variable and flux, respectively, given by

$$\mathbf{U} = \begin{pmatrix} \rho \\ \rho u \\ \rho v \\ \rho w \\ e \end{pmatrix}, \mathbf{F} = \begin{pmatrix} \rho u \\ \rho u^2 + p \\ \rho uv \\ \rho uw \\ (e+p)u \end{pmatrix}, \mathbf{G} = \begin{pmatrix} \rho v \\ \rho vu \\ \rho v^2 + p \\ \rho vw \\ (e+p)v \end{pmatrix}, \mathbf{E} = \begin{pmatrix} \rho w \\ \rho wu \\ \rho wv \\ \rho w^2 + p \\ (e+p)w \end{pmatrix}, \tag{2}$$

where primitive variables in the unknown $\mathbf{U}$ are density ρ, velocity components u, v and w, respectively, total energy per unit volume e, and fluid pressure p. The total energy e is related to the equation of state by

$$e = \frac{p}{\gamma - 1} + \frac{\rho}{2}(u^2 + v^2 + w^2), \tag{3}$$

where γ, the specific heat ratio, is taken as 1.4 in the present computation.

3   Numerical Methods

The explicit difference equations of (1) discretized in space by using the dispersion-controlled scheme (Jiang et al. 1995) are given as

$$\left(\frac{\partial \mathbf{U}}{\partial t}\right)^n_{i,j,k} = -\frac{1}{\Delta x}(\mathbf{H}^n_{i+\frac{1}{2},j,k} - \mathbf{H}^n_{i-\frac{1}{2},j,k}) - \frac{1}{\Delta y}(\mathbf{P}^n_{i,j+\frac{1}{2},k} - \mathbf{P}^n_{i,j-\frac{1}{2},k})$$

$$-\frac{1}{\Delta z}(\mathbf{Q}^n_{i,j,k+\frac{1}{2}} - \mathbf{Q}^n_{i,j,k-\frac{1}{2}}) \qquad (4)$$

with

$$\begin{cases} \mathbf{H}^n_{i+\frac{1}{2},j,k} = \mathbf{F}^+_{i+\frac{1}{2}L,j,k} + \mathbf{F}^-_{i+\frac{1}{2}R,j,k} \\ \mathbf{P}^n_{i,j+\frac{1}{2},k} = \mathbf{G}^+_{i,j+\frac{1}{2}L,k} + \mathbf{G}^-_{i,j+\frac{1}{2}R,k} \\ \mathbf{Q}^n_{i,j,k+\frac{1}{2}} = \mathbf{E}^+_{i,j,k+\frac{1}{2}L} + \mathbf{E}^-_{i,j,k+\frac{1}{2}R} \end{cases} , \qquad (5)$$

where the $(\cdot)^+$ or $(\cdot)^-$ superscript denotes flux splitting according to the Steger and Warming method, and more detailed introduction to the scheme was described by Jiang et al. 1995. Numerical solutions were marched in time by using the Runge-Kutta algorithm of second-order accuracy. Reflecting boundary conditions were specified both on solid walls and the planes of symmetry. Non-reflecting boundary conditions were applied at inflow and outflow boundaries. Computations were carried out in one quarter of the domain as shown in Fig. 1 because of the symmetric assumption. The equally-spaced grid of $600 \times 150 \times 150$ mesh points was used in case 1,2 and 3, and 50×50 points were distributed along the cross section of the shock tube. In case 3, the grid is composed of $400 \times 180 \times 120$ mesh points and 60×40 points were in the cross-section. Several view directions for observations are also defined in Fig. 1, which are the side view, the corner view; the back view, the front view, the diagonal plane and the mid-wall symmetrical plane.

4   Results and Discussion

Four test cases are carried out by discharging shock waves from the open end of shock tubes into ambient air for different Mach number measured before the shock waves move out of the shock tubes. In the discussion below, four main physical processes are emphasized, which are the secondary flow motion; secondary shock wave generation; axis-switching and the role of aspect ratio in axis-switching. These processes are self-induced flow motions closely linked to non-circular jet instability and have no relation to any disturbance in background flows.
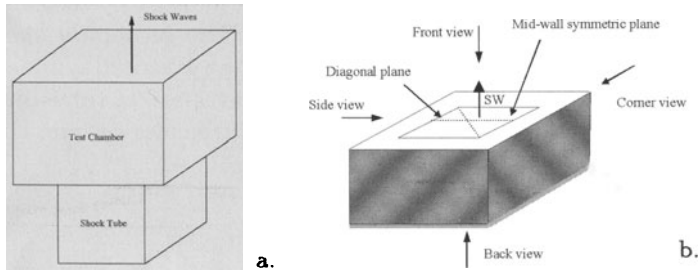

Fig. 1. Schematic of computational domain and view directions for flow visualization
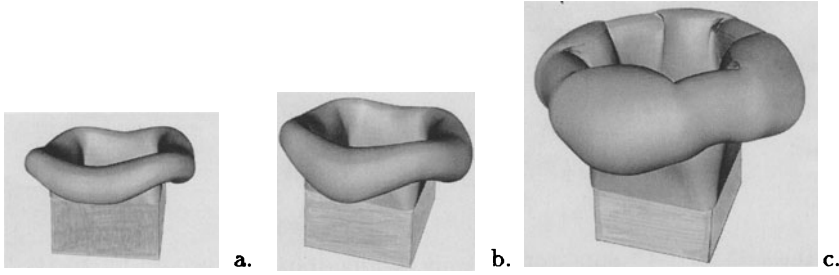
Fig. 2. Distortion of the primary vortex loop due to secondary flow shown with the iso-vorticity surface for $M_s = 1.29$: **a.** $t = 200\ \mu s$; **b.** $t = 300\ \mu s$; **c.** $t = 500\ \mu s$

4.1   Secondary Flow Motion

Numerical results of case 1 is calculated for $M_s = 1.29$ in a square cross-section shock tube. Three sequential three-dimensional displays of iso-vorticity surface are presented. Figure 2a shows the starting of the secondary flow motion. The flow fronts can be observed in the primary vortex loop that undergoes a diameter change. In this stage, straight parts of the primary vortex loop, not affected by the secondary flows, are still observable nearby the mid-wall symmetrical plane, but are shortened with an increase in loop diameter. The larger diameter of the primary vortex loop is observable in Fig. 2b, which indicates that the secondary flows imploded in the mid-wall symmetrical plane and will move back again to corners. Generally speaking, once the transmitting shock wave is discharged from the open end of a shock tube, the secondary flows will develop at shock tube corners due to the non-uniform expansion, move to the mid-wall symmetric plane, and finally result in jet instability as shown in Fig. 2c.

4.2   Secondary Shock Waves

The second case is similar to the first case but for a higher Mach number of 1.5. A special feature observable is some discontinuities in the iso-vorticity surface, as shown in Fig. 3b. These iso-vorticity surfaces appears very smooth in its earlier stages as shown in Fig. 3a. The discontinuities are induced by secondary shock waves due to locally-developed supersonic flows. The secondary shock waves appear earlier near the corner plane and then do in the mid-wall symmetric plane somewhere downstream. Therefore, these shock waves are of three-dimensional characters and can impose three-dimensional disturbances on non-circular jet flows as shown in Fig. 3c.

4.3   Axis-Switching of the Primary Vortex Loop

Figure 4 shows results of case 3. The primary vortex loop from the corners of the shock tube exit moves further downstream whereas other parts of the primary vortex loop in the mid-wall symmetrical plane do so more in the radial
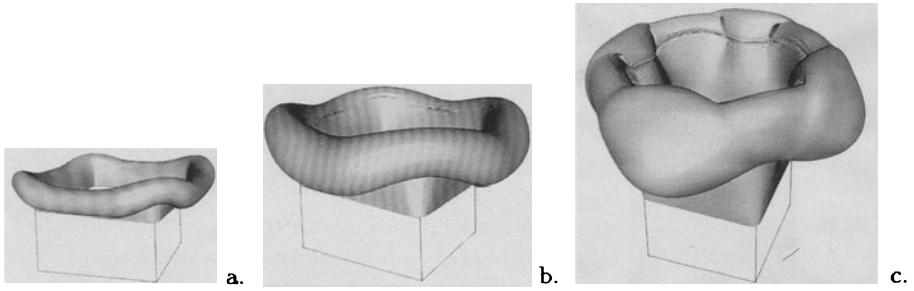
Fig. 3. Disturbances due to secondary shock waves shown with the iso-vorticity surface for $M_s = 1.5$: **a.** $t = 146$ μs; **b.** $t = 386$ μs; **c.** $t = 536$ μs
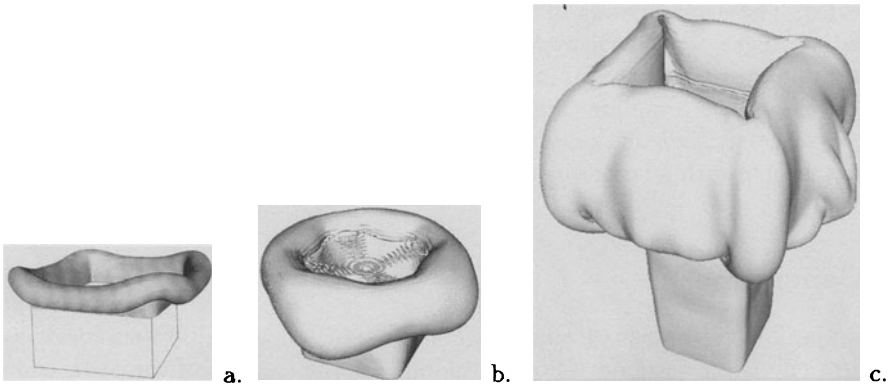

Fig. 4. Axis-switching of non-circular jets shown with the iso-vorticity surface for $M_s = 1.5$: **a.** $t = 146$ μs; **b.** $t = 450$ μs; **c.** $t = 737$ μs

direction, as shown in Fig. 4a. This is the so-called flow spreading. The flow expansion at the corners is stronger than that in the mid-wall symmetric plane due to diffraction of the transmitting shock wave. Actually, the expansion process in the diagonal plane appears similar to axis-symmetric cases whereas that in the mid-wall symmetrical plane has a somewhat two-dimensional characteristics. Therefore, the primary vortex loop is generated with non-uniform vorticity distribution, which is considered to be self-induced and an intrinsic character of non-circular jets. The larger diameter of the primary vortex loop is observable in Fig. 4b, and the first 45° axis-switching is completed. Figure 4c shows the further deformation of the primary vortex loop, and the second phase of the axis-switching is finished. The first phase of axis-switching can be explained with flow expanding but the second phase cannot be. Therefore, the secondary flow motion may be the driving force for the second phase of axis-switching.
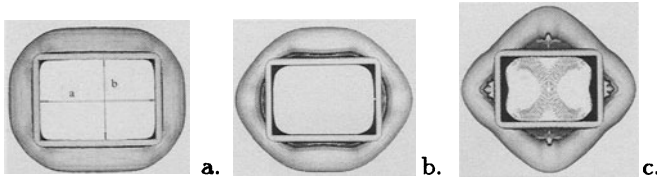
Fig. 5. Back views of the primary vortex loop shown with the iso-vorticity surface for $M_s = 1.5$ and aspect ratio 1.5: **a.** $t = 140\ \mu s$; **b.** $t = 310\ \mu s$; **c.** $t = 466\ \mu s$

4.4   Role of Aspect Ratio

The last case is similar to case 3, but the shock tube is rectangular not square. The aspect ratio of the shock tube is 1.5 and Mach number was taken to be $M_s = 1.5$. Three back views of the primary vortex loop deformation at three sequential stages are shown with the iso-vorticity surface in Fig. 5. From this figure it was observed that within the first 45° axis-switching, the primary vortex loop develops into a square one. If comparing with the results in case 3 the more asymmetrical vorticity distribution is predicted here. This may imply that rectangular jets with a large aspect ratio will develop more easily into instability.

5   Conclusions

Two major flow phenomena leading to non-circular jet instability were identified. The first one is the secondary flow developing at the corners of the open end of shock tubes and moving down along the primary vortex loop. This motion results from asymmetrical pressure and vorticity distributions, and plays an important role in the axis-switching of the primary vortex loop. It is also a key driving force that leads to the deformation of the primary vortex loop and the development of hairpin vortices and coherence structures. The other is the secondary shock wave that is generated due to locally-developed supersonic flows and induces three-dimensional disturbances. These two physical phenomena are self-induced and considered to be the intrinsic characters of non-circular jets.

References

1. H.S. Husain and F. Hussain: J. Fluid Mech, **248**, (1993)
2. S.H. Lee, I.S. Jeung and Y. Yoon: AIAA Journal, **36**, (1998)
3. G. Raman: Physics Fluids, 11, (1998)
4. G.Raman and R. Taghavi: J. Fluid Mech, **354**, (1998)
5. S. Koshigoe, E. Gutmark and K.C. Schadow: AIAA Journal, 27,(1989)
6. A. Krothapalli, D. Baganoff and K. Karamcheti: J. Fluid Mech, **170**,(1981)
7. Z. Jiang, K. Takayama and Y.S. Chen: Comp Fluid Dynamics J, **2**, (1995)
8. O. Onodera, Z. Jiang and K. Takayama: JSME Int J **41**, (1998)
9. G. Raman: J. Fluid Mech, **330**(1997)
10. C.K.W. Tam and A.T. Thies: J. Fluid Mech, **248**, (1993)